

EXPERIMENTAL MEASUREMENTS OF MICROFRACTURE IN CEMENT-BASED MATERIALS

E. N. Landis

University of Maine, Orono, Maine, USA

S. P. Shah

Northwestern University, Evanston, Illinois, USA

Abstract

Acoustic emission techniques were used to monitor microfracture in cement-based materials. The goals of this research were to characterize microcracking in cement-based materials of varying composition, to track the evolution of damage in these materials, and to examine the relationships to overall fracture behavior. Microcracking in coarse mortar, fine mortar, cement paste, and DSP cement paste were monitored using quantitative acoustic emission analysis. Microcracks were characterized according to their fracture mode. Characterizations of the microcracks showed a relationship between the degree of inhomogeneity in the material and the microfracture mode. The fine-grained materials tested showed primarily mixed mode microfracture, whereas the microfracture in the coarse-grained materials had a larger mode II (shear) component. The overall fracture toughness of the different materials were also measured and compared to microfracture mode.

1 Introduction

The fracture behavior of concrete is often attributed to a fracture process zone. This fracture process zone manifests itself in the nonlinear stress-strain behavior, post peak strain softening, size effect, and various toughening mechanisms. Features of the fracture process zone include arrays of microcracks, aggregate interlocking, crack bridging, and grain boundary sliding friction. From a material modeling standpoint, properties of the fracture process zone must be known in order to accurately predict the response of the material to stress. Since the fracture process zone characteristics are critical to material performance, a better understanding of those characteristics will lead to a better understanding of overall performance.

In order to investigate some of the microstructural phenomena which make up the fracture process zone, an experimental program using quantitative acoustic emission techniques was conducted. The specific goals of the program were to evaluate microcrack properties through the deconvolution of recorded AE waveforms, and to examine the relationship between the recovered microcrack properties and the overall fracture properties of the material. To this end a series of plain (unreinforced) beam specimens were tested in three point bending under closed-loop control. The microcracking was monitored using an array of acoustic emission transducers.

2 Background

Acoustic emission is a nondestructive test method for evaluating damage growth in materials. An acoustic emission (AE) is the spontaneous release of localized strain energy in a material. This energy release causes the propagation of stress waves which can be detected at the surface of the material. Acoustic emissions result from microcracking, dislocation movement, and other irreversible changes. The nature of damage in the material can be deduced through an analysis of detected AE waveforms. Acoustic emissions are typically monitored using highly sensitive piezoelectric transducers connected to data amplification and recording instrumentation.

Analysis of AE phenomena can range from relatively simple counting of AE events, analysis of energy or frequency, and locating AE sources (Miller and McIntire, 1987), to more sophisticated quantitative AE analysis (Hsu et al. 1977). AE techniques have been applied to concrete for a number of years. Diederichs et al. compiled a particularly

extensive review of conventional AE applications to concrete. Included in their review are the effects of loading devices, specimen size, aggregates, ultimate strength, and temperature on the AE counts and frequency spectra. More recent work has focused on relating acoustic emission characteristics to properties of the fracture process zone (e.g. Rossi et al. 1989, Maji et al. 1990, Niiseki et al. 1992). AE source location analysis has also been applied to crack localization (Li and Shah 1994) and crack tip measurements (Chen et al. 1992) in concrete. Quantitative AE analysis has been used to evaluate cracking from anchor bolt pull-out (Ohtsu et al. 1991). The advantage of AE measurement techniques is the ability to monitor microscopic damage occurring *inside* the material *while it is occurring*.

Traditional analysis of AE data involves the recording of event rates, peak amplitudes, frequency spectra, and source locations. Empirical relationships can be made with damage growth or other observed phenomena. Although this type of analysis can provide valuable insight into fracture behavior, a more sophisticated analysis is necessary for characterization of the actual microfracture event which caused the acoustic emission. Hsu et al. (1977) established a *quantitative* acoustic emission model where the AE event is broken down into three separate processes: (1) the source (microcrack) event, (2) the resulting stress wave propagation through the material, and (3) the measurement of the waveform on the specimen surface. These three processes are assumed to be linear systems so that they may be combined through a series of convolutions as (Michaels et al. 1981):

$$V(t) = T(t) * \{G(t) * M(t)\} \quad (1)$$

where $V(t)$ is the voltage measured from an AE transducer, $M(t)$ is a function representing the AE source, $G(t)$ accounts for the wave propagation through the material, $T(t)$ is the response function of the AE transducer. "*" denotes a convolution integral. Through an inverse analysis, the characteristics of an AE source can be determined from the measured voltage transients if the response of the transducer, and the wave propagation characteristics of the material are known.

The solution to the AE inverse problem is presented in Landis and Shah 1993. A brief summary is presented here.

The AE (microcrack) source is represented by a seismic moment tensor which equates the microcrack discontinuity with a set of equivalent body forces. This equivalence may be written (Aki and Richards 1980):

$$M_{ij} = C_{ijkl} b_k n_l \Delta A \quad (2)$$

Here $b_k n_l \Delta A$ is discontinuity with area, ΔA , and slip direction, b_k . The plane of the discontinuity has a normal vector n_l . C_{ijkl} is the elastic stiffness tensor, and M_{ij} is the seismic moment tensor. For isotropic materials eq. (2) can be simplified to:

$$M_{ij} = \left[\lambda b_k n_k \delta_{ij} + \mu (b_i n_j + b_j n_i) \right] \Delta A \quad (3)$$

where λ and μ are the Lamé constants. Microcrack parameters of orientation, volume and slip angle can be determined from the principal values and principal directions of M_{ij} . If the principal values of M_{ij} are denoted by $M^{(1)}$, $M^{(2)}$, and $M^{(3)}$, and the principal directions are denoted by $\mathbf{x}^{(1)}$, $\mathbf{x}^{(2)}$, and $\mathbf{x}^{(3)}$, then the microcrack orientation, volume and slip angle can be defined by (Enoki and Kishi 1988):

$$n_i = \frac{1}{2(b_k b_k)^{1/2}} (x_i^{(1)} - x_i^{(3)}) \quad (4)$$

$$V = b_k n_k \Delta A = \frac{M^{(1)} + M^{(2)} + M^{(3)}}{3\lambda + 2\mu} \quad (5)$$

$$\cos \alpha = \frac{b_k n_k}{(b_k b_k)^{1/2}} = \frac{2\mu M^{(2)}}{\lambda (M^{(1)} - M^{(3)})} \quad (6)$$

where \mathbf{n} is a vector normal to the crack plane, V is the microcrack volume, and α is the angle between \mathbf{n} and the direction of motion between the two faces of the microcrack, b_k . Using this designation, and angle of α close to 0° indicates mode I (tensile) microcracking, whereas an angle of α close to 90° indicates mode II (shear) microcracking. Thus, through the use of equations (4)-(6), a microcrack may be uniquely characterized in terms of its volume, orientation, and slip angle.

The moment tensor components are determined through an inversion of equation (1). The theoretical basis for equation (1) is an integral solution of the differential equation of motion in an elastic solid. The far field displacement u_i , in an elastic medium at point \mathbf{x} , due to a transient dipole body force M_{jk} , acting at point ξ can be written:

$$u_i(\mathbf{x}, t) = \int_{-\infty}^{\infty} G_{ij,k}(\mathbf{x}, \xi, t - \tau) M_{jk}(\xi, \tau) d\tau \quad (7)$$

where $G_{ij,k}$ is the elastodynamic Green's function for the medium. Since equation (7) is a convolution integral, $G_{ij,k}$ may be thought of as the response of the medium at \mathbf{x} , due to an impulse load (both spatial and temporal) applied at ξ . If equation (7) is convolved with the impulse response function for the AE transducer, the result is equation (1). Thus, if the Green's function for the medium, and the transducer response function are known, then moment tensor representing a microcrack can be determined through an inversion of equation (7) at a number of locations.

A nonlinear least-squares approach was developed for the required multichannel inversion (Landis and Shah 1993). The multichannel inversion produces the nine moment tensor components. The moment tensor is then rotated to its principal axes. Finally, the microcrack parameters (orientation, volume and slip angle) are evaluated using equations (4) through (6).

3 Experimental program

An experimental program was carried out to examine the relationship between the microfracture characteristics and the overall mechanical response of the material. In order to make this examination, specimens of different microstructural characteristics were tested. The properties of the specimens as well as the types of tests conducted are described below.

A series of three point bend specimens of varying composition were cast for this program. The specimens were designated as follows: coarse mortar, fine mortar, plain cement paste, and DSP cement paste. The fine mortar had a maximum aggregate size of 1 mm, and the coarse mortar had a maximum aggregate size of 5 mm. The results of previous experiments showed that the "coarse mortar" represents the practical limit of quantitative AE analysis of microcracking in cement-based materials (Landis 1993). The proportion of aggregate in the mortars was 2 parts aggregate to 1 part cement. The DSP cement paste is a portland cement-based material with a very low water-cement ratio, and a relatively large fraction of added silica fume. After the constituents are thoroughly mixed, a vacuum is applied to minimize the amount of entrapped air. The result is a material with a very dense microstructure (as compared to conventional cement-based materials). All of the specimens were demolded approximately 24 hours after casting, and were placed in a water bath for curing.

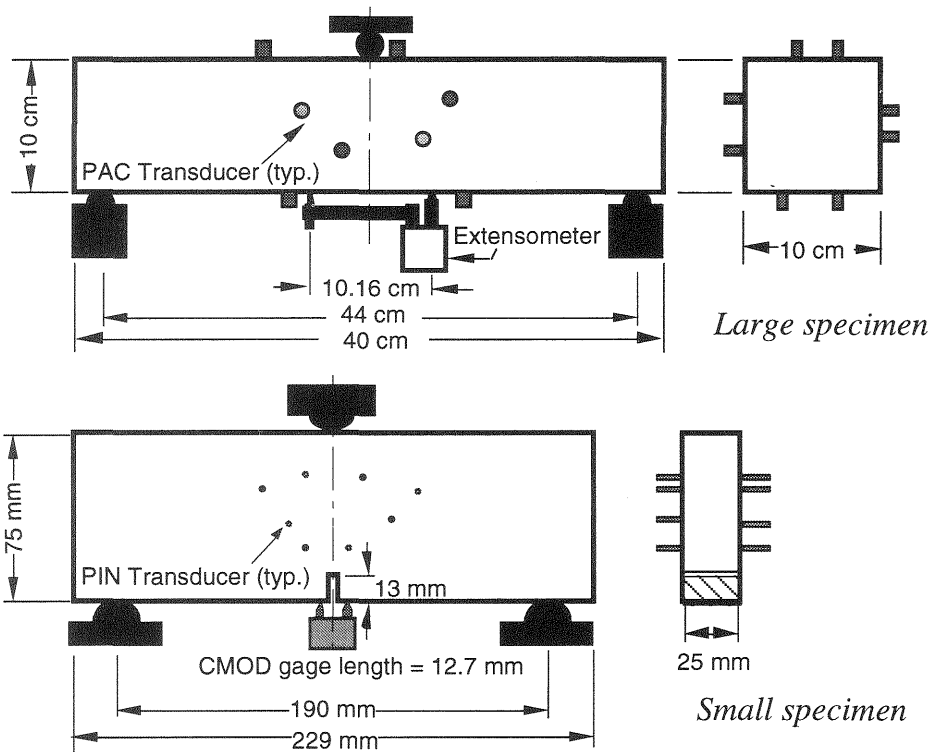


Fig. 1. Specimen geometries

Two different sized specimens were tested. The specific specimen geometries are shown in Figure 1. Three large specimens were tested: coarse mortar, fine mortar, and normal cement paste. Two small specimens were tested: DSP paste, and normal cement paste. The smaller size was chosen for the DSP specimen because of the difficulty in properly casting larger DSP specimens. A small normal cement paste specimen was also tested so that there would be a common reference for both sizes, eliminating any possible size-related bias in the measurement system.

All specimens were tested in a closed-loop, servo-hydraulic load frame. The experimental setup is illustrated in Figure 2. The closed-loop feedback parameter for the large specimens was the tensile strain as measured by a 4 inch extensometer mounted on the bottom of the beam. For the small specimens a center notch was cut in the beams and a gage was placed over the notch for crack mouth opening displacement (CMOD) measurements. The CMOD measurement was used as the feedback control.

The specimen loading rate was programmed such that the displacement gages would open at a rate of 5.0×10^{-5} mm per second for

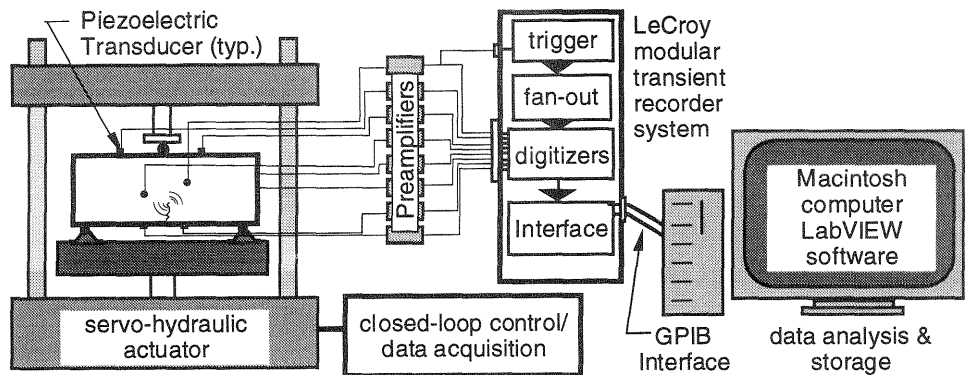


Fig. 2. Experimental setup

the large specimens, and 3.5×10^{-5} mm per second for the small specimens.

The components of the AE measurement system are illustrated in Figure 2. A LeCroy modular transient recorder system was used to acquire the AE waveforms. A LabVIEW-based application was developed to record the signals and to control the LeCroy system. For all tests eight channels of AE data were recorded. The length of the data record for each channel was 1024 points. The sampling rate of the transient recorders was 16 MHz, for the large specimens and 32 MHz for the small specimens.

Two different types of piezoelectric transducers were used. These transducers were the model micro80 AE transducer manufactured by Physical Acoustics Corp (PAC), and the model CA-1135 position transducer (PIN) manufactured by Dynasen Inc. Each of the transducers were calibrated against a glass capillary reference signal. The PIN transducers were found to have a more broadbanded displacement response than the PAC transducers. However, the PAC transducers were much more sensitive up to about 250 kHz (Landis 1993). The PAC transducers were used on the larger specimens because of their better sensitivity.

4 Experimental results

The cumulative AE event counts are plotted along with the loads for the two paste specimens in Figures 3 and 4. The event counts shown in these figures illustrate an interesting characteristic of the AE properties of cement-based materials. This characteristic is that the rate of AE activity appears to increase just prior to the ultimate load. In the cement paste specimen (Fig 3), the increase in event rate occurs at the peak load. The

obvious differences between the materials. The microcracks in the mortars tend to be mostly in the range of $10,000 \mu\text{m}^3$ whereas the paste specimens tend to have more cracks in the range of $20,000 \mu\text{m}^3$. The volumes recovered are a measure of the energy release of the microcrack since it is a function of the principal moment tensor values and the elastic properties. It is not, however necessarily a good indication of the area or opening of a microcrack since these values are indeterminate.

The recovered slip angles for each specimen are shown in Figure 8. The slip angle, α was defined as the angle between a vector normal to the microcrack plane, and a vector representing the direction of crack motion of one face relative to the other. The majority of the microcrack slip angles recovered for the two mortar specimens tend to be relatively close to 90° , indicating a dominance of shear microfracture modes. There is a significant difference in the slip angles of the paste specimens. Both show much larger crack opening components (smaller slip angles). Although the shear component in both of these is still fairly high (a majority of normal paste events had slip angles in the 70° to 75° range while the DSP had the most events in the 65° to 70° range), it seems clear that the nature of the microcracking is different in the fine versus the coarse-grained materials.

A plot of the recovered microcrack volumes and the corresponding load is shown in Figure 9 for the coarse mortar specimen. Figure 10 shows the slip angles and load history. It can be seen in these figures that there are likely different modes of microfracture at different points on the loading cycle. This could represent microcracking in different material phases. Microcracks occurring early in the loading cycle have often been attributed to primarily matrix-aggregate interface cracks. As load approaches the peak the microcracking also includes the matrix phase (Slate and Hover 1984). If it is assumed that matrix cracking consists of a higher energy release than interface cracking, then Figure 9 shows that there is primarily matrix cracking around the peak load, whereas the strain softening region could primarily be interface cracking. If this is the case, then from Figure 10 it could be concluded that the matrix cracking is predominantly mixed mode, whereas the interface cracking is primarily shear. This theory could be supplemented by the fact that both cement paste specimens showed primarily mixed mode microcracking.

6 Comparison to fracture toughness

The fracture toughness of the materials tested was measured using the two parameter fracture model (RILEM 1990). Tests on the DSP and cement

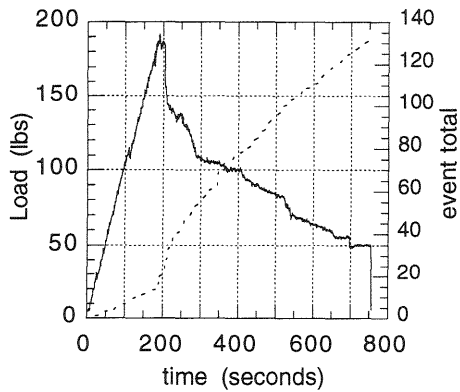


Fig 3. Paste load and event count

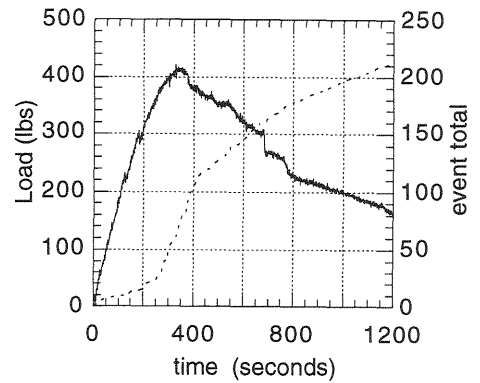


Fig. 4 DSP load and event count

specimen also shows linear prepeak behavior. In the DSP specimen (Fig 4) the event rate jump occurs at about 86% of the peak. There is a notable nonlinear prepeak region in this specimen.

Li and Shah (1994) attributed this jump in the AE event rate to the localization of microcracking in to a single critical crack. In their specimens of mortar and concrete the jump occurred typically at about

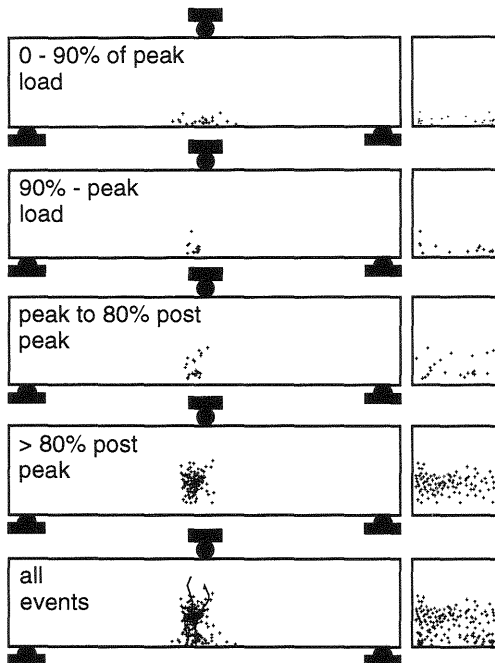


Fig. 5 AE source locations, coarse mortar specimen

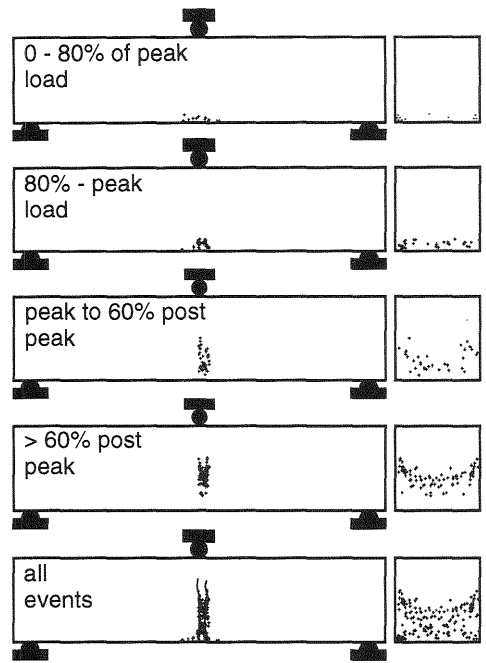


Fig. 6 AE source locations fine mortar specimen

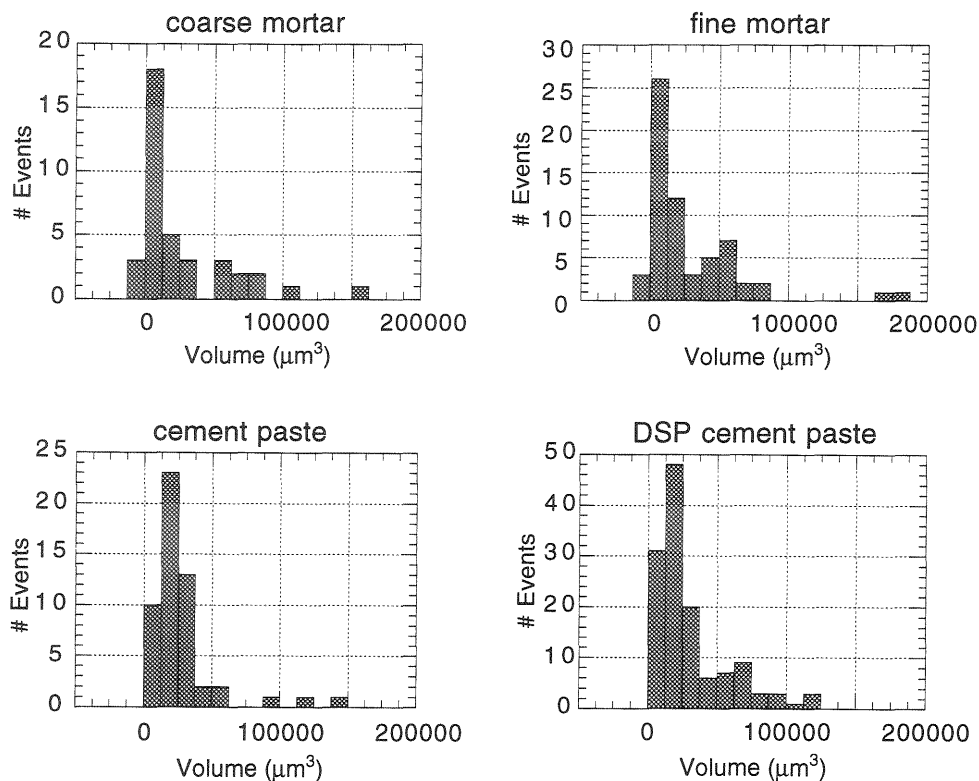


Fig. 7 Histograms of microcrack volumes

80% of the peak load. Ohtsu (1989) attributed the AE event rate increase to the formation of the fracture process zone. He also suggested that a linear elastic fracture mechanics (LEFM) approach could be applied to concrete if the load for evaluating fracture toughness was taken as the load where the AE event rate jumps and the fracture process zone forms.

The locations of the AE sources were evaluated according to the methods described in Landis et al (1992). The source locations evaluated in the coarse and fine mortar specimens are shown at four different stages in Figures 5 and 6 respectively. In each of these figures the initial AE source locations are distributed over a relatively wide area in the zone of maximum tensile stress. Prior to peak load, the AE events tend to localize into a zone close to the observed surface crack. Nearly all subsequent AE events are confined to this narrow band.

The recovered microcrack volumes were calculated for each specimen and are plotted in Figure 7. There does not appear to be any

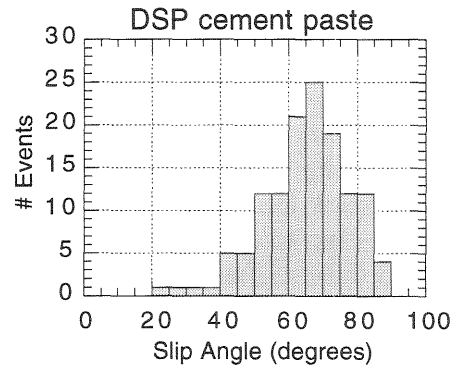
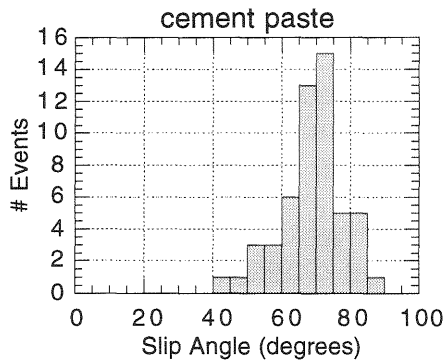
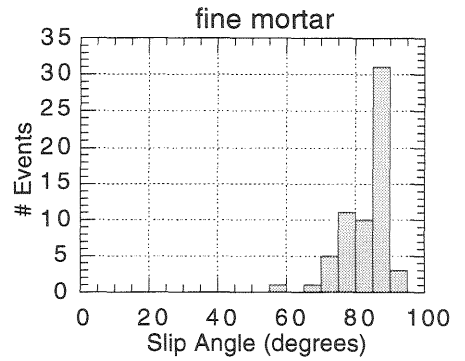
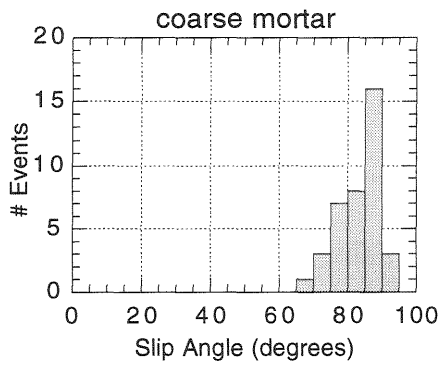


Fig. 8 Histograms of microcrack slip angles

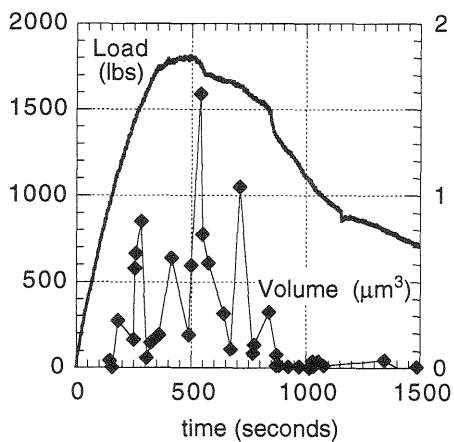


Fig. 9 Load and μ crack volumes coarse mortar specimen

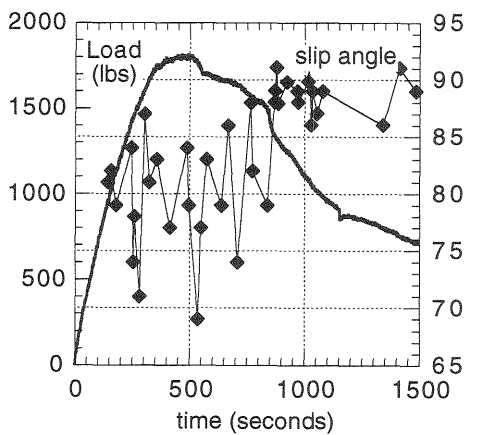


Fig. 10 Load and slip angles coarse mortar specimen

Table 1 Measured fracture parameters

Material	K_{Ic} (KPa \sqrt{m})	CTOD _c (mm)	a_c (mm)	average α (deg)
coarse mortar	703	.0046	21.6	83.3
fine mortar	727	.0053	21.6	83.7
normal paste	380	.0041	17.36	64.8, 66.1 ¹
DSP paste	717	.0033	17.09	68.6

¹ the first value was calculated from the large paste specimen and the second from the small paste specimen

paste specimens were conducted as a part of this experimental program. Fracture toughness values for the fine and coarse mortar specimens were taken from published tests of comparable materials (Jenq and Shah 1985). The values of fracture parameters used in this analysis are shown in Table 1.

The measured critical effective crack length a_c was compared to the average slip angle α measured in each specimen. These two values are plotted in Figure 11. Although there are not enough data points for a statistically significant relationship, but the figure shows an apparent relationship between the average microcrack slip angle and the critical effective crack length.

A similar relationship can be established between the average slip angle and the roughness of the fractured surfaces (Landis 1993).

7 Conclusions

It is apparent from the results of this investigation that quantitative AE analysis yields a wealth of information about microcracking and

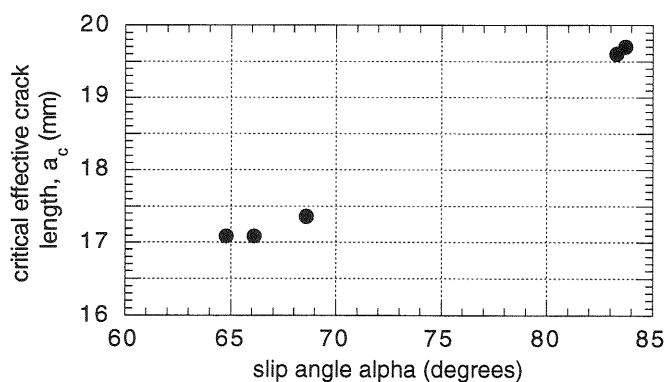


Fig. 11 Critical Effective Crack Length versus microcrack slip angle

microfracture processes. The AE event rate, the source locations, and the microcrack parameters all can be synthesized to aid in the understanding of microcracking and its role in mechanical behavior. In this paper, the rate of AE activity was shown to correspond to nonlinearities in the load-CMOD curves. AE source were shown to localize prior to the peak load in the specimens. Microcrack volumes did not vary significantly between different specimens, but slip angles did. The mortar specimens showed a much higher shear component microfracture component than did the paste specimens. The progression microcrack characteristics along the load cycle for the specimens illustrates that interface cracks could likely be the source of the high shear component microcracks. It was also shown that there seems to be a direct relationship between average microcrack slip angle and the critical effective crack length of the material. If the shear microcracks are attributed to grain boundary sliding and other frictional mechanisms, then the much of the increase in fracture toughness (as indicated by the critical effective crack length) of the coarse-grained materials over the fine-grained materials can be attributed to these energy absorbing mechanisms.

In summary, the results of the tests conducted as a part of this research program can be used to infer properties of the fracture process zone as well as the specific characteristics of individual microcracks. The properties of the microcracks can ultimately be linked to the overall fracture behavior of the materials.

Acknowledgments

The authors wish to acknowledge the support of the Air Force Office of Scientific Research and the program manager Dr. Spencer T. Wu, and the NSF Center for Advanced Cement-Based Materials at Northwestern University.

References

- Aki, K. and Richards, P.G. (1980) **Quantitative Seismology, Theory and Methods**. W.H. Freeman, New York, chapters 2-4.
- Chen, H.L., Cheng, C.T. and Chen S.E. (1992). Determination of fracture parameters of mortar and concrete beams by using acoustic emission. **Materials Evaluation**, 50(7), 888-894.
- Diederichs, U., Schneider, U. and Terrien M. (1983) Formation and propagation of cracks and acoustic emission. in **Fracture Mechanics of Concrete**, (ed F.H. Wittmann), Elsevier Science Publishers B.V., Amsterdam.

- Enoki, M., and Kishi, T. (1988) Theory and analysis of deformation moment tensor due to microcracking. **International Journal of Fracture**, 38, 295-310.
- Hsu, N.N., Simmons, J.A. and Hardy S.C. (1977). An approach to acoustic emission signal analysis. **Materials Evaluation**, 35, 100-106.
- Jenq, Y.-S., and Shah, S.P. (1985) A fracture toughness criterion for concrete. **Engineering Fracture Mechanics**, 21, 1055-1069.
- Landis, E.N., Ouyang, C., and Shah, S.P. (1992) Automated determination of first P-wave arrival and AE source location. **Journal of Acoustic Emission**, 10, S97-S103.
- Landis, E.N. (1993) A quantitative acoustic emission investigation of microfracture in cement-based materials. Ph.D. Dissertation, Department of Civil Engineering, Northwestern University, Evanston, Illinois.
- Landis, E.N., and Shah, S.P. (1993) Recovery of microcracking in mortar using quantitative acoustic emission. **Journal of Nondestructive Evaluation**, 12, 219-232.
- Li, Z., and Shah, S.P. (1994) Microcracking in concrete under uniaxial tension. **ACI Materials Journal**, 91(4), 372-381.
- Michaels, J.E., Michaels, T.E., and Sachse, W. (1981) Applications of deconvolution to acoustic emission signal analysis. **Materials Evaluation**, 39, 1032-1036.
- Miller, R.K.; McIntire, and P. Editors (1987) **Nondestructive Testing Handbook: Volume 5, Acoustic Emission Testing**, ASNT.
- Niiseki, S.; Mihashi, H., and Nomura, N. (1992) Relationship between fracture toughness and widths of fracture process zones in mortar and concrete analyzed by improved AE source location, in **Progress in Acoustic Emission VI**, The Japanese Society for NDI, Tokyo, 463-470.
- Ohtsu, M. (1989) AE application to fracture mechanics. **JCI Transactions**, 11, 673-678.
- Ohtsu, M., Shigeishi, M., Iwase, H. and Koyangi, W. (1991) Determination of crack location, type and orientation in concrete structures using acoustic emission. **Magazine of Concrete Research**, 43, 127-134.
- RILEM Committee on Fracture Mechanics of Concrete - Test Methods (1990) Determination of fracture parameters (K^S_{IC} and $CTOD_C$) of plain concrete using three-point bend tests. **Materials and Structures**, 23, 457-460.
- Rossi, P., Robert J.L., Gervais J.P., and Bruhat D. (1989) Identification of the physical mechanisms underlying acoustic emissions during the cracking of concrete. **Matériaux et Constructions**, 22, 194-198.
- Slate, F.O., and Hover, K.C. (1984) Microcracking in Concrete. in **Fracture Mechanics of Concrete: Material Characterization and Testing**, (eds. Carpinteri, A.; Ingrassia, A.R.), Martinus Nijhoff: Boston, 137-160.